High Aspect Ratio Silicon Dioxide-Coated Single-Walled Carbon Nanotube Scanning Probe Nanoelectrodes

Yoshie Narui, Donato M. Ceres, Jinyu Chen, Konstantinos P. Giapis,* and C. Patrick Collier*,†

Division of Chemistry and Chemical Engineering, California Institute of Technology, Pasadena, California 91125

Received: February 5, 2009; Revised Manuscript Received: February 20, 2009

We have fabricated high aspect ratio, hydrophilic nanoelectrodes from individual single-walled carbon nanotubes (SWNTs) mounted on conductive atomic force microscope (AFM) tips for use as electrochemical probes. Individual SWNTs with an average diameter of 5 nm and up to 1.5 μm in length were passivated with nanometer-thick SiO_2 films, deposited conformally in an inductively coupled plasma reactor. The electrically insulating SiO_2 films improved the nanotube rigidity and stabilized the nanotube−AFM tip contact to enable use in aqueous environments. The nanotube tip was successfully exposed by subjecting the probe to nanosecond electrical pulse etching but only after electron beam irradiation in a transmission electron microscope (TEM). Probe functionality was verified by electrodepositing gold nanoparticles from aqueous solution only at the exposed tip.

Introduction

Carbon nanotubes attached to scanning probes have been widely used for structural and functional imaging purposes.[1] Because of the small diameter and high aspect ratio of the nanotube, these modified probes have excellent lateral resolution and are able to probe deep crevices.[2] In addition, the end of the nanotube can be covalently modified to facilitate studies of chemical and biological interactions on surfaces.[3,4] Single-walled carbon nanotubes (SWNTs) behave as one-dimensional wires that are either metallic or semiconducting.[5] Their mechanical strength and wear-resistance has made SWNTs ideal candidates for use in scanning probe lithography and data storage.[6−8] SWNTs selectively grown on scanning probes have been used to achieve extremely high bit density for improved data storage capability.[7] In electrochemical systems, nanoelectrodes are subject to enhanced mass transport because of the dominance of radial diffusion at nanometer dimensions, thereby increasing the faradaic to charging current ratio.[9] In addition, carbon nanotube-based electrodes have demonstrated enhanced electrocatalytic performance relative to other materials, including other forms of carbon, because of defect sites along the walls and at open ends of the nanotubes, allowing for more efficient electrical transfer with electroactive species in solution and faster electrochemical kinetics.[10] When combining the high aspect ratio and conductivity of SWNTs with the high spatial resolution of scanning probes, it is possible to design a point-source sensor or a localized trigger for electrochemical reactions in aqueous nanoenvironments. An electrically contacted SWNT with well-defined geometry represents an ideal nanoelectrode, but the fabrication of such a tool is nontrivial.[11]

Lieber and co-workers were the first to mount SWNTs onto atomic force microscope (AFM) probes by using an adhesive and subsequently functionalizing the nanotubes with phenyl and amine groups.[3] These probes were used to measure adhesion forces on self-assembled monolayer surfaces but were not used as nanoelectrodes. Because of the lateral flexibility of individual SWNTs, the protrusion length of the mounted nanotubes extending from the AFM tip support had to be shortened by electrical pulse etching to less than 100 nm. Rinzler et al. attached multiwalled carbon nanotubes (MWNTs) onto tips and coated the entire assembly with Parylene C.[12] After laser exposure of the nanotube, its electrical conductivity was characterized using scanning conductance microscopy, but detailed electrochemical characterization of the probe in solution was not performed. More recently, Macpherson et al. utilized SWNTs as templates to fabricate gold disk nanoelectrodes embedded in poly(oxyphenylene) and silicon nitride.[13] These well-defined nanoelectrodes were successfully used for high resolution electrochemical and topographical imaging. However, the electrode diameter was determined by the deposited gold layer and not the SWNT diameter, with a significant reduction in the probe aspect ratio.

The fabrication of SWNT nanoelectrodes for use in aqueous media must meet several critical challenges: (1) good electrical contact between the SWNT and the AFM tip must be maintained, (2) the entire probe must be chemically passivated and electrically insulated, while the electrochemical activity is limited to the end of the exposed nanotube tip, and (3) the insulating layer must improve the mechanical strength of the nanotube and reinforce the contact between probe and nanotube to survive repeated immersion into aqueous environments.

Our previous work demonstrated the fabrication of well-defined, highly conductive nanoelectrodes using a fluorocarbon coating.[14] However, because of the strongly hydrophobic nature of the film, these SWNT probes could not be submerged into aqueous media without damage or loss of the attached nanotube. We report here on a method to produce conformal hydrophilic coatings of silicon oxide (SiO_2) on carbon nanotubes using plasma-assisted decomposition of tetraethyl orthosilicate (TEOS) at low pressure. We demonstrate the suitability of high aspect ratio SiO_2-coated SWNT probes for use in aqueous environments. Furthermore, we present a high-voltage (HV) pulse

* To whom correspondence should be addressed. (K.P.G.) E-mail: giapis@cheme.caltech.edu, phone: (626) 395-4180, fax: (626) 568-8743; (C.P.C.) e-mail: colliercp@ornl.gov, phone: (865) 576-3638, fax: (864) 574-1753.

† Current address: Oak Ridge National Laboratory, Center for Nanophase Materials Sciences, Oak Ridge, TN 37831.

10.1021/jp901080e CCC: $40.75
Published on Web 03/27/2009

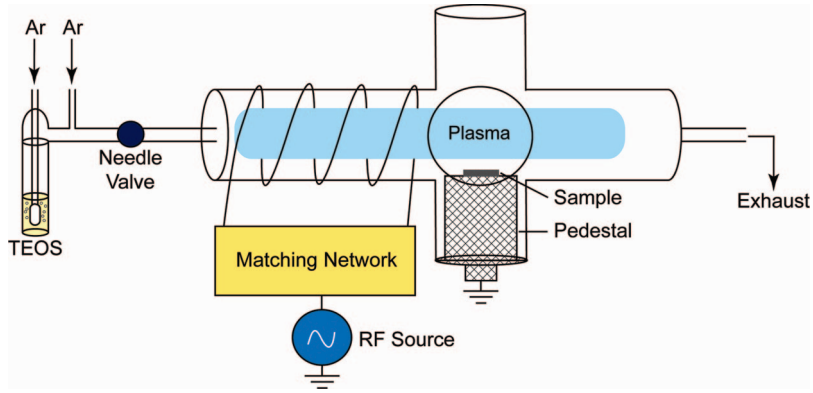

Figure 1. Schematic of the inductively coupled plasma reactor. Typical conditions for conformal coating of the tip assemblies were 6.375 sccm Ar (bubbled through TEOS), 1.125 sccm Ar only, reactor pressure = 120 mTorr, rf power = 100 W, deposition duration 60 to 180 s.

etching technique to expose the apex of the coated SWNT for potential use as a nanoelectrode or for further functionalization.

Experimental Methods

A Digital Instruments Multimode AFM with a Nanoscope IV controller was used for this work. All experiments were conducted with the AFM shielded in a Faraday cage. TEM images of the scanning probes were taken with a Phillips EM420 microscope operating at 120 kV. Metal films (10 nm Cr, 75 nm Au) were thermally evaporated onto AFM probes (Multi75, Budget Sensors) twice with a 180° rotation to ensure uniformity of metalization. As-grown SWNTs were attached to Au-coated AFM tips using the pick-up technique developed by Lieber and co-workers.[15] SWNTs with an average diameter of 5 nm (determined by TEM) were grown by chemical vapor deposition as described previously.[16] The length of the protruding nanotubes varied from 250 nm to 2 μm. After attachment of the nanotube, the tips were annealed under an inert argon atmosphere for 1 h at 190 °C to improve electrical contact with the gold.

SiO_2 deposition onto the scanning probes was performed in a home-built inductively coupled plasma (ICP) reactor. The reactor assembly, schematically shown in Figure 1, consists of a six-way Pyrex glass chamber (i.d. 100 mm) with an upstream extension tube to accommodate a 4-turn copper tube antenna. Power was supplied to the antenna from a 1000 W radio frequency power supply at a fixed frequency of 13.56 MHz. A conventional π-network matchbox was used to ensure precise impedance matching. The reactor was supplied with a pure argon flow, while a second argon line was bubbled through liquid TEOS maintained at 20 °C. The combined flows were introduced into the reactor through a needle valve, which served to prevent uncontrolled boiling of TEOS. Multiple probes were assembled with the nanotubes pointing up on an aluminum holder, which was in good electrical contact with a pedestal connected externally to the network matchbox ground.

The SiO_2 film properties were characterized after depositing layers on planar model substrates of silicon (100), polycrystalline Au, and highly ordered pyrolytic graphite (HOPG), because of their similarities to the AFM probe and SWNT surfaces. Film thicknesses were determined using a Gaertner L116C ellipsometer operating at $\lambda = 632.8$ nm. Topography and surface roughness of the films were analyzed using tapping mode AFM.[17] The chemical composition of the deposited films was determined by X-ray photoelectron spectroscopy (XPS), carried out in an ultrahigh vacuum chamber on an M-probe surface spectrometer described in detail elsewhere.[18] Electrochemical impedance spectra were collected with a Solartron impedance analyzer in the frequency range of 0.1 Hz to 50 kHz.

A nanosecond HV-pulse etching method was used to remove the SiO_2 located at the apex of a fully insulated SWNT probe. The pulse was applied when the tip was within a few nanometers from a grounded platinum surface. The probes were mounted into an electrostatic force microscopy (EFM) tip holder, which allowed for the direct application of voltage to the tip. The separation distance between the tip and the surface (z-position) was controlled by a feedback loop in force calibration mode. Using a signal access module (break-out box), the low voltage z-position signal was monitored with an SR 830 lock-in amplifier, which triggered an Agilent 33220A waveform generator. When the nanotube was within a few nanometers of the platinum surface, the waveform generator triggered an Agilent 8114A pulse generator to apply a 100 ns pulse to the tip. The applied potential was varied until a significant change in the z-position was observed.

The insulating properties of the SiO_2 coatings were assessed electrochemically by immersing the AFM cantilever-tip assembly in aqueous solution containing reduced ferrocenylmethyl-trimethylammonium ($FcTMA^+$) and hexafluorophosphate (PF_6^-) counterions, with KCl as a supporting electrolyte. $FcTMA^+$ was selected for its chemical stability, and its frequent use as an electrochemical standard.[19,20] Cyclic voltammograms (CVs) of the nanoelectrodes were collected in a solution of 2 mM $FcTMA^+$ at varying scan rates with an EG&G/Princeton Applied Research 173 potentiostat. The setup included an Ag/AgCl reference electrode and a platinum counter electrode. The current was measured at the working electrode with a Keithley 6514 electrometer, and all data were collected with a Tektronix TDS 2012B storage oscilloscope. Gold was formed electrochemically on the exposed SWNT nanoelectrodes immediately after pulse etching using a solution of 4 mM $HAuCl_4$ in 0.1 M KCl. The electrochemical cell described below was used to apply a reducing potential of −200 mV for an interval of 100 ms.

In addition, the nanoelectrodes were characterized using a procedure reported by Wilson et al. for analyzing electrically connected, uncoated SWNT conducting probe tips.[11] Briefly, a 100 μm diameter hemisphere of mercury was formed in situ by the reduction of Hg^{2+} with NO_3^- counterions at a platinum disk ultramicroelectrode. This served as the liquid metal contact for the SWNT nanoelectrode. The probe approached the mercury drop in tapping mode until the drop was penetrated by the nanotube. At a fixed z-displacement, current−potential (IV) curves were recorded where only the nanotube portion of the tip was immersed in the mercury. IV curves were collected before and after pulse etching to determine if the nanotube tip was exposed.

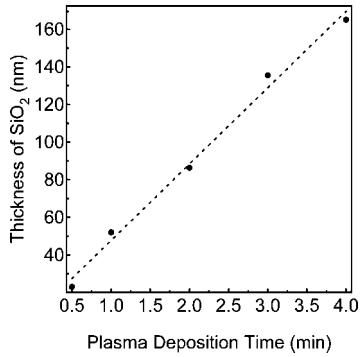

Figure 2. Variation in SiO_2 film thickness on polycrystalline gold as a function of deposition time at a constant plasma power of 75 W.

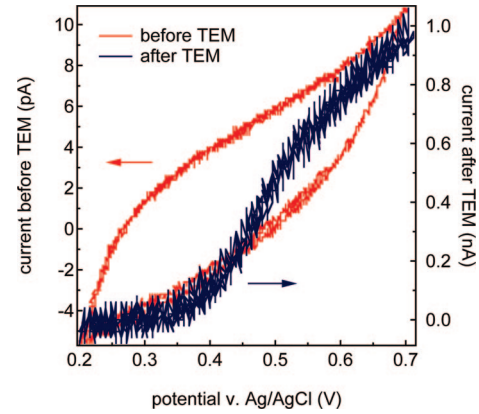

Figure 3. Cyclic voltammagram with $FcTMA^+$ of a SWNT-attached gold-coated AFM probe passivated with 60 nm of SiO_2 before (left arrow) and after (right arrow) TEM imaging. The scan rate was 10 mV/s.

Results and Discussion

As shown in Figure 1, SiO_2 deposition was performed on a grounded stage at ambient temperature located in the plasma afterglow region, to protect the SWNTs from bombardment of ions generated in the plasma. The main advantage of this plasma coating process is the ability to generate precursors under mild conditions which can effectively polymerize as a SiO_2 film onto the nanotube tip. Figure 2 shows that the film thickness on a flat surface varies linearly with time up to 4 min with no limiting processes evident. AFM images of the planar substrates showed the coated surfaces to be conformal with an rms roughness of 1.5 and 0.9 nm for Au and HOPG surfaces, respectively (see Supporting Information). XPS analysis revealed that the ratio of oxygen to silicon was 2.05, near the expected composition ratio for SiO_2. The resistivity and dielectric constant of the thin SiO_2 layer were determined by impedance spectroscopy to be 1.3×10^{11} Ω·m and 2.7, respectively. The resistivity for high quality SiO_2 films (300 nm to 50 μm thickness) used in microelectronics applications has been reported to range from 10^{12} to 10^{14} Ω·m, and the dielectric constant ranges from 3.9 to 4.2.[21] The lower resistivity and dielectric constant of the TEOS plasma-deposited SiO_2 is attributed to residual carbon present in the film due to incomplete fragmentation of TEOS in the plasma.

Following plasma deposition of SiO_2, the insulating ability of each scanning probe was electrochemically tested in $FcTMA^+$ solution. In all cases, the nanotubes remained attached to the AFM tip, because of the mechanical reinforcement of the connection between the gold-coated probe and the SWNT from the hydrophilic SiO_2 layer. Nanoelectrodes that could survive repeated immersion in aqueous solution without damage or alteration of the insulating properties of the SiO_2 coating required SWNTs no longer than 1.5 μm, and a minimum SiO_2 film thickness of 30 nm. When the SWNT length exceeded 1.5−2 μm, the nanotube tended to buckle and break open the thin oxide layer (see Supporting Information).

Figure 3 shows that background currents for coated nanotube probes that had not been pulse etched were dominated by capacitive charging effects and were below 10 pA, with no faradaic peaks observed. We were unable to confirm faradaic currents from exposed SWNT tips with cyclic voltammetry (CV) in "blind" measurements (i.e., no previous TEM imaging); either faradaic currents from opened nanotube tips were overwhelmed by capacitive charging, or the pulse etching process resulted in loss of the electrical contact between the nanotube and the conductive AFM tip. Probes that were imaged by TEM but were not HV-pulse-etched to expose the tip showed significantly larger amounts of leakage current (hundreds of pA) that was faradaic. We attribute the sharp increase in current for potentials above 0.4 V to oxidation of $FcTMA^+$ (formal potential 0.42 V vs Ag/AgCl). Included in the Supporting Information are CVs taken before and after TEM exposure of a SiO_2-coated AFM tip without an attached SWNT that shows similar behavior. On the basis of this and other observations described below, we believe the AFM tip support, and not the coated SWNT probe, is the dominant source of this faradaic leakage current.

The electron beam used during TEM imaging clearly modifies the SiO_2 film properties to cause a noticeable change in the observed insulating behavior. It is known that SiO_2 films become unstable under intense electron irradiation,[22] and at high enough levels, SiO_2 can become mobile or lose oxygen content.[23−25] While leakage in the passivating layer should be avoided, electron bombardment seems to be essential for successful HV-pulse etching of the tip. For example, the probe shown in Figure 4a was coated with 60 nm of SiO_2 and pulsed up to +100 V without exposing the tip before TEM imaging. Nanotube tips without TEM exposure could be opened by HV-pulse etching, but generally at much higher voltages than imaged tips, frequently causing damage to the sidewalls. After TEM imaging, the probe of Figure 4a was etched by applying only +25.2 V, which shortened the probe length as shown in Figure 4b. Similar behavior was observed for over 30 tips. Clearly, electron beam irradiation during imaging of the probe affected the dielectric strength of the SiO_2 coating.

While TEM images visibly show that the end of the SiO_2 coating has been removed, further evidence was needed that the exposed nanotube tip was conductive. This was corroborated by immersing the end of the tip into a mercury drop and collecting IV curves after HV-pulse etching. Before pulse etching, the coated probes exhibit no conductivity. After pulse etching, the IV curves showed a highly symmetric response with a low-bias ohmic resistance of 200 kΩ as inferred from Figure 4c, consistent with the presence of a metallic nanotube.[11] This indicates that the SiO_2 film did not affect the SWNT−gold AFM tip contact resistance or inherent electrical properties of the nanotube and that the pulse etching only removed the film from the end of the nanotube.

In addition to metallic nanotubes, other assembled nanoelectrodes consisted of picked-up SWNTs demonstrating semiconducting behavior. The IV traces of these nanoelectrodes were asymmetric and nonlinear, with a resistance of ~5 MΩ at low bias (data not shown). This result is consistent with the uncoated semiconducting nanotubes described by Wilson et al.[11] and with semiconducting nanotubes coated with fluorocarbon films and

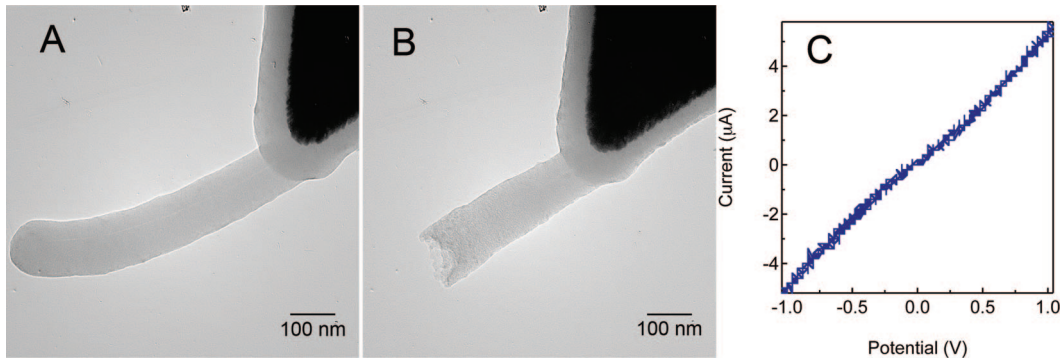

Figure 4. (A) Fully insulated SWNT nanoelectrode coated with 60 nm of SiO_2 and electrically pulsed at voltages up to +100 V. (B) The same probe etched with a +25.2 V pulse after electron beam irradiation. (C) An IV curve for the etched probe in B taken after immersion in a 100-μm diameter mercury drop.

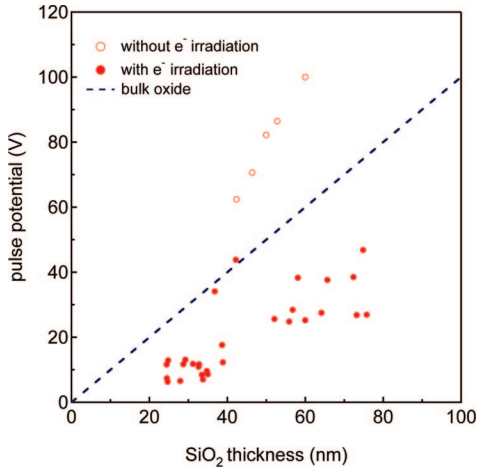

Figure 5. The pulse potential required to open fully insulated nanoelectrodes plotted as a function of SiO_2 thickness. The dashed line represents the dielectric strength (V/nm) of high quality SiO_2 thin films.

exposed by pulse etching described by us.[14] The mercury drop method provided a straightforward means of identifying metallic or semiconducting probes. For use as a nanoelectrode, metallic SWNTs are preferred for their lower resistance over a wide potential window. Finally, it is important to note that nanotubes are also susceptible to damage by electron irradiation starting at 86 kV.[26] However, because the resistance values and IV curve trends of exposed SiO_2-coated SWNT probes were consistent with previous studies of uncoated nanotube probes,[11] the electron damage was presumably localized to the outer oxide layer.

There was a statistically significant difference in the voltage required to HV-pulse etch nanotubes of SiO_2-coated nanoelectrodes, which had been first imaged by TEM as compared to those that had not. The pulse voltage required to expose the nanotube tip as a function of SiO_2 thickness from 34 probes is plotted in Figure 5. The blue dashed line corresponds to the literature value for the dielectric strength of high-quality SiO_2 thin films (10^7 V/cm).[27] For electrodes that were not preimaged by TEM, the voltage required to open the tips was higher than the literature value, and had a steeper slope. This was likely because of a high contact resistance between the tip and the platinum substrate when pulsing during tapping mode operation. Less than optimal orientation of the nanotube probe to the platinum surface resulted in an increase in the voltage necessary to reach breakdown. For nonimaged tips, the breakdown voltage for opening the tips scaled linearly with film thickness, while for imaged tips it is not clear there is such a linear trend. The precise mechanism behind the electron beam-facilitated opening of these probes is still unclear, though the random formation of minute point defects in the film is suspected.

To further demonstrate that only the end of the nanotube was exposed by the nanosecond pulse etching process, gold was electrochemically reduced onto the nanotube in aqueous solution. This technique has previously been used to create metal nanowires through the potentiostatic reduction of noble metals onto the ends and sidewalls of carbon nanotubes.[28,29] Figure 6 shows a TEM-imaged tip coated with 65 nm SiO_2 before and after applying a pulse of +37.6 V at the tip. The final image shows that a gold plug has formed where the SiO_2 film had been previously removed. Gold nanoparticle formation was not observed on the SiO_2-coated nanotube sidewalls or AFM tip support. This result confirmed that the SWNT maintained electrical contact with the gold-coated AFM probe. In addition, the pulse etching process succeeded at removing the coating only at the very end of the tip without irreparably damaging the conductivity of the nanotube. Finally, the electrochemically active area is clearly confined to the tip apex and not the sidewall regions of the probe, which indicates that the insulating SiO_2 film conformally coats the SWNT sidewalls and is sufficiently thick to prevent electron transfer. This suggests that the main source of the background faradaic currents in the electrochemical measurements of TEM imaged probes in Figure 3 was not the SiO_2-coated nanotube region of the probe but the SiO_2−Au-coated AFM tip assembly, which has a much larger surface area. The estimated surface area of the SiO_2-coated nanotube is approximately 0.21 μm^2 while for the AFM tip assembly the area is 3500 μm^2.

The diffusion-limited steady-state current for an exposed carbon nanotube tip in 2 mM $FcTMA^+$ solution can be estimated by approximating the exposed tip as a 2.5 nm radius disk electrode with the expression $i_{lim} = 4naFDc$, where n is the number of transferred electrons, a is electrode radius, F is the Faraday constant, D is the diffusion coefficient of the redox mediator (7.5×10^{-6} cm^2/s), and c is its concentration.[30] From this calculation, leakage currents will have to be reduced to about 1 pA in order to detect faradaic currents uniquely at the exposed nanotube tip.

While HV-pulse etching of electron-irradiated probes is more consistent and reproducible than nonirradiated probes, it does not work for all the probes with the same degree of success. Alternative processes for removing the SiO_2 film at the tip apex such as chemical etching (with HF) and focused ion beam milling have been considered but were not successful. The most promising albeit time-consuming method tried was mechanical abrasion of the tip by repeatedly scanning the tip in contact mode on a rough, conductive diamond surface.[31] This method

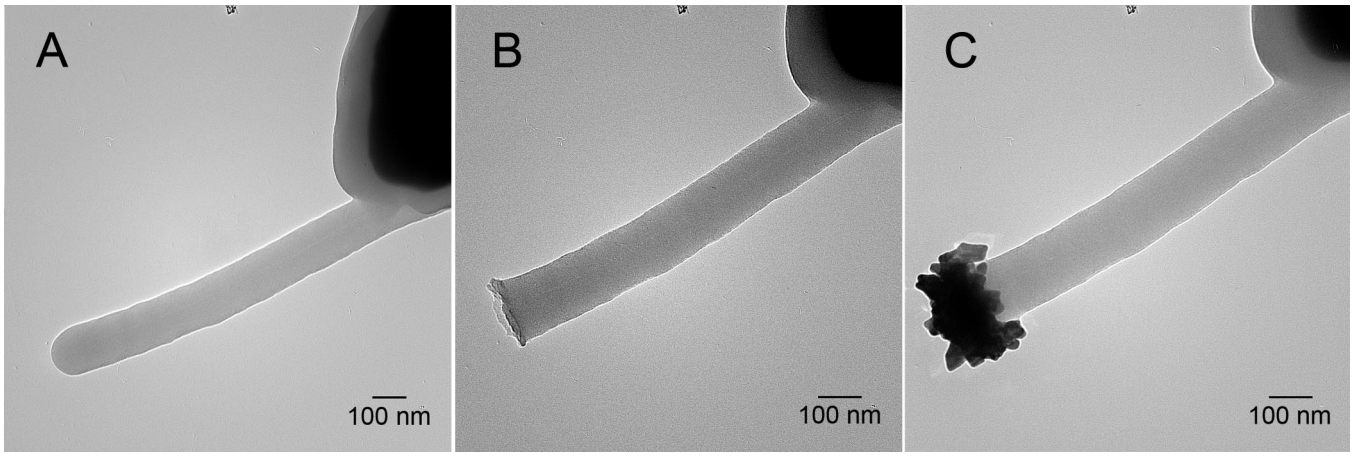

Figure 6. Fully insulated SiO_2 coated SWNT nanoelectrode (A) before and (B) after applying a +37.6 V pulse at the tip. (C) Gold nanoparticle electrochemically reduced onto the exposed nanotube from a solution of $AuCl_4^-$ held at −200 mV for 200 ms.

produced wear-tolerant "nanopencils," which have been successfully tested as conductive probes in air but not solution. The fine resolution of the SWNT at the core of the nanopencil was successfully demonstrated by writing (and subsequently reading) inverted domain dots as small as 6.8 nm in diameter on ferroelectric films of epitaxial lead zirconate titanate.[31]

Conclusions

A reliable fabrication method for high aspect ratio SiO_2-coated SWNT scanning probes for potential use as biological nanoelectrodes has been developed and characterized. SWNTs, up to 2 μm in length, were mounted on gold-coated AFM scanning probes and passivated with a minimum of 30 nm of a plasma-deposited SiO_2 dielectric thin film. In all cases, the coated nanotubes survived immersion in water. TEM imaging preceded by a HV-pulse etching technique was used to remove a small portion of SiO_2 located at the very end of the nanotube. The bare nanotube was conductive and electrochemically active as demonstrated by reduction of gold ions from solution and nanoparticle formation onto the exposed probe tip. Because of capacitive charging and background leakage currents from the AFM tip support, faradaic currents have yet to be measured from the exposed SWNT. Capacitive charging effects can be circumvented by integrating current over time at fixed potentials using chronocoulometry.[32] Decreasing the carbon content in the plasma-deposited films, for example with addition of oxygen in the plasma, will result in SiO_2 films with improved insulating and dielectric properties. This should enable the use of thinner SiO_2 layers that can be pulse-etched at the SWNT tip in air, without the need for electron beam-induced modification and the resulting leakage currents from the probes when immersed in solution. The measurement of faradaic currents from exposed SWNT tips would confirm that fully functional nanoelectrodes have been obtained. Such scanning probe tips would be indispensable for probing fundamental questions of chemistry and biology at the nanoscale.

Acknowledgment. The authors thank Carol Garland for assistance with TEM imaging. Nicholas Brunelli provided invaluable expertise with the ICP reactor. This work was supported by Arrowhead Research and Intel Corporation.

Supporting Information Available: SiO_2 thickness measurements by ellipsometry, topographical images by AFM, resistance and capacitance measurements by electrochemical impedance spectroscopy, chemical composition by XPS, synthesis of ferrocenylmethyl-trimethylammonium hexafluorophosphate, CVs taken before and after TEM exposure of a SiO_2-coated AFM tip without an attached SWNT, TEM images of electrochemically formed gold particles on SiO_2-coated probes that were pulse-etched but had not been exposed to an electron beam, and TEM images of long SWNTs (2 μm length, not pulse-etched) that had buckled and broken through the thin oxide layer. This material is available free of charge via the Internet at http://pubs.acs.org.

References and Notes

(1) Hafner, J. H.; Cheung, C. L.; Woolley, A. T.; Lieber, C. M. *Prog. Biophys. Mol. Biol.* **2001**, *77*, 73.
(2) Dai, H. J.; Hafner, J. H.; Rinzler, A. G.; Colbert, D. T.; Smalley, R. E. *Nature* **1996**, *384*, 147.
(3) Wong, S. S.; Woolley, A. T.; Joselevich, E.; Cheung, C. L.; Lieber, C. M. *J. Am. Chem. Soc.* **1998**, *120*, 8557.
(4) Wong, S. S.; Joselevich, E.; Woolley, A. T.; Cheung, C. L.; Lieber, C. M. *Nature* **1998**, *394*, 52.
(5) Saito, R.; Dresselhaus, G.; Dresselhaus, M. S. *Physical Properties of Carbon Nanotubes*; Imperial College Press: London, 1998.
(6) Ishikawa, K.; Honda, K.; Cho, Y. *Nanotechnology* **2007**, *18*, 084015.
(7) Cooper, E. B.; Manalis, S. R.; Fang, H.; Dai, H.; Matsumoto, K.; Minne, S. C.; Hunt, T.; Quate, C. F. *Appl. Phys. Lett.* **1999**, *75*, 3566.
(8) Dai, H. J.; Franklin, N.; Han, J. *Appl. Phys. Lett.* **1998**, *73*, 1508.
(9) Arrigan, D. W. M. *Analyst* **2004**, *129*, 1157.
(10) Nugent, J. M.; Santhanam, K. S. V.; Rubio, A.; Ajayan, P. M. *Nano Lett.* **2001**, *1*, 87.
(11) Wilson, N. R.; Cobden, D. H.; Macpherson, J. V. *J. Phys. Chem. B* **2002**, *106*, 13102.
(12) Patil, A.; Sippel, J.; Martin, G. W.; Rinzler, A. G. *Nano Lett.* **2004**, *4*, 303.
(13) Burt, D. P.; Wilson, N. R.; Weaver, J. M. R.; Dobson, P. S.; Macpherson, J. V. *Nano Lett.* **2005**, *5*, 639.
(14) Esplandiu, M. J.; Bittner, V. G.; Giapis, K. P.; Collier, C. P. *Nano Lett.* **2004**, *4*, 1873.
(15) Hafner, J. H.; Cheung, C. L.; Oosterkamp, T. H.; Lieber, C. M. *J. Phys. Chem. B* **2001**, *105*, 743.
(16) Wade, L. A.; Shapiro, I. R.; Ma, Z. Y.; Quake, S. R.; Collier, C. P. *Nano Lett.* **2004**, *4*, 725.
(17) Horcas, I.; Fernandez, R.; Gomez-Rodriguez, J. M.; Colchero, J.; Gomez-Herrero, J.; Baro, A. M. *Rev. Sci. Instrum.* **2007**, *78*, 013705.
(18) Haber, J. A.; Lewis, N. S. *J. Phys. Chem. B* **2002**, *106*, 3639.
(19) Heller, I.; Kong, J.; Heering, H. A.; Williams, K. A.; Lemay, S. G.; Dekker, C. *Nano Lett.* **2005**, *5*, 137.
(20) Lemay, S. G.; van den Broek, D. M.; Storm, A. J.; Krapf, D.; Smeets, R. M. M.; Heering, H. A.; Dekker, C. *Anal. Chem.* **2005**, *77*, 1911.
(21) Miller, R. D. *Science* **1999**, *286*, 421.
(22) Ajayan, P. M.; Iijima, S. *Philos. Mag. Lett.* **1992**, *65*, 43.
(23) Chen, G. S.; Boothroyd, C. B.; Humphreys, C. J. *Philos. Mag. A* **1998**, *78*, 491.

(24) Storm, A. J.; Chen, J. H.; Ling, X. S.; Zandbergen, H. W.; Dekker, C. *J. Appl. Phys.* **2005**, *98*, 014307.

(25) Storm, A. J.; Chen, J. H.; Ling, X. S.; Zandbergen, H. W.; Dekker, C. *Nat. Mater.* **2003**, *2*, 537.

(26) Smith, B. W.; Luzzi, D. E. *J. Appl. Phys.* **2001**, *90*, 3509.

(27) Sze, S. M. *Semiconductor Devices, Physics and Technology*; Wiley: New York, 1985.

(28) Choi, H. C.; Shim, M.; Bangsaruntip, S.; Dai, H. J. *J. Am. Chem. Soc.* **2002**, *124*, 9058.

(29) Quinn, B. M.; Dekker, C.; Lemay, S. G. *J. Am. Chem. Soc.* **2005**, *127*, 6146.

(30) Campbell, J. K.; Sun, L.; Crooks, R. M. *J. Am. Chem. Soc.* **1999**, *121*, 3779.

(31) Tayebi, N.; Narui, Y.; Chen, R. J.; Collier, C. P.; Giapis, K. P.; Zhang, Y. G. *Appl. Phys. Lett.* **2008**, *93*, 103112.

(32) Steel, A. B.; Herne, T. M.; Tarlov, M. J. *Anal. Chem.* **1998**, *70*, 4670.

JP901080E